Journal of Solid State Chemistry **158,** 218–226 (2001)
doi:10.1006/jssc.2001.9095, available online at http://www.idealibrary.com on IDEAL®

New Antimony Lanthanide Disulfide Dibromides $LnSbS_2Br_2$ (Ln = La, Ce): Crystal and Electronic Structures and Optical Properties

D. Gout, S. Jobic,[1] M. Evain, and R. Brec

Institut des Matériaux Jean Rouxel, UMR 6502, Laboratoire de Chimie des Solides, BP 32229, 44322 Nantes Cedex 3, France

Received September 12, 2000; in revised form January 2, 2001; accepted January 19, 2001; published online March 27, 2001

$CeSbS_2Br_2$ (I), $Ce_{1/2}La_{1/2}SbS_2Br_2$ (II), and $LaSbS_2Br_2$ (III) have been synthesized at 700°C from a mixture of $LnBr_3$, Ln_2S_3, Sb, and S and characterized by single-crystal X-ray diffraction. The three phases are isostructural (space group $P2_1/c$, $Z = 4$) and crystallize in a novel, dense, bidimensional structure with cell parameters $a = 8.709(3)$ Å, $b = 9.187(2)$ Å, $c = 17.397(5)$ Å, $\beta = 104.26(3)°$ for I, $a = 8.739(7)$ Å, $b = 9.219(7)$ Å, $c = 17.41(2)$ Å, $\beta = 104.3(1)°$ for II, and $a = 8.785(1)$ Å, $b = 9.236(2)$ Å, $c = 17.372(3)$ Å, $\beta = 104.09(2)°$ for III. In these compounds, $[LnS_5Br_4]$ and $[LnS_3Br_6]$ (Ln = Ce, La) distorted tricapped trigonal prisms define infinite $^2_\infty[LnS_2Br_2]$ layers counterbalanced and capped by antimony cations. In good accordance with the structural features, the charge balance in these materials is to be written $Ln^{III}Sb^{III}S_2^{-II}Br^{-I}$. These compounds exhibit a yellow hue with a measured absorption threshold of 2.42(1), 2.55(1), and 2.72(1) eV for I, II, and III, respectively. In the two cerium containing bromothioantimonates I and II, the origin of the color is assigned to a Ce–4f → Ce–5d electronic transition, which shifts to higher energy from I to II due either to a matrix effect (increase of the mean Ln–S distances under the substitution of Ce for La) or to an atomic ordering between Ce and La cations on the Ln(1) and Ln(2) crystallographic sites. In contrast, the electronic transition at play in III involves a charge transfer from the bromine and sulfur ions to the antimony ions, the latter contributing substantially to the lowermost levels of the conduction band. © 2001 Academic Press

Key Words: **antimony lanthanide disulfide dibromide; crystal structure; optical properties; electronic structure; color origin; cerium; lanthanum.**

INTRODUCTION

Recently, $Ce_3(SiS_4)_2I$ was synthesized, its crystal structure determined, and its luminescence properties evidenced (1, 2). Indeed, this material appears very interesting in view of its original structural arrangement and its physical characteristics. First, its tridimensional structure, containing novel $[CeS_8I]$ building blocks which self assemble, allows us to envision the development of a new, rich structural chemistry related to an expected large diversity of conceivable $[LnS_uX_v]$ polyhedra (Ln = lanthanide, X = Cl, Br, I) with various potential connectivities. Second, this material exhibits a strong room temperature luminescence in the blue region of the visible spectrum associated to a Ce^{III}–$5d^1 \rightarrow Ce^{III}$–$4f^1$ radiative de-excitation (2). Thanks to the ability of iodine atoms to be substituted for Cl and Br, $Ce_3(SiS_4)_2Br$ and $Ce_3(SiS_4)_2Cl$ were also prepared. These materials, isostructural to their heavier congener, showed slightly different chromatic properties. In fact, the Ce–4f/Ce–5d energy separation determined from diffuse reflectance measurements decreases from 2.92 to 2.82 eV and to 2.72 eV going from iodine to bromine and to chlorine. This trend has been supported by emission experiments carried out at 300 K making clear a change of the $5d^1 \rightarrow 4f^1$ energy gap. Hence, $Ce_3(SiS_4)_2I$ and $Ce_3(SiS_4)_2Br$ fluoresces in the blue, while $Ce_3(SiS_4)_2Cl$ fluoresces in the green. This change in energy of the 4f–5d separation must be ascribed to an inductive effect of the halogenide on the Ce–S bond (3–5): the more ionic the Ce–X bond, the more covalent the Ce–S bond and the lower the $4f^1 \rightarrow 5d^1$ energy separation. This suggests that other halosulfides containing cerium may present tunable chromatic and luminescence properties. This tunability prompted us to investigate the Ce/MG/S/X systems (MG: main group element, X = Cl, Br, I), and in particular the Ce/Sb/S/Br system. We reported recently the synthesis and the characterization of Ce_2SbS_5Br, $CeLaSbS_5Br$, and La_2SbS_5Br, red materials (6) with a novel structural arrangement, for which the coloration does not involve the commonly expected Ce–$4f^1 \rightarrow$ Ce–$5d^1$ absorption mechanism but stems from the promotion of an electron from the top of the valence band toward the conduction band, i.e., from unpaired S and/or Br toward Sb and/or paired S. We present here the synthesis and characterization of $CeSbS_2Br_2$, $Ce_{1/2}La_{1/2}SbS_2Br_2$, and $LaSbS_2Br_2$, materials with colors ranging from bright to pale yellow.

[1] To whom correspondence should be addressed. E-mail: jobic@cnrs-imn.fr.

0022-4596/01 $35.00

EXPERIMENTAL

Synthesis

$Ce_{1-x}La_xSbS_2Br_2$ compounds ($x = 0$, 0.5, and 1) were prepared from $CeBr_3$ and $LaBr_3$ (Cerac, 99.9%), Ce_2S_3 and La_2S_3 (Cerac, 99.9%), antimony (Aldrich, 99.995%), and sulfur (Aldrich, 99.998%) weighted in the Ce : La : Sb : S : Br elemental ratios 2 : 0 : 1 : 3.5 : 2 for $CeSbS_2Br_2$ (**I**), 1 : 1 : 4 : 10 : 2 for $Ce_{1/2}La_{1/2}SbS_2Br_2$ (**II**) and 0 : 1 : 1 : 2 : 2 for $LaSbS_2Br_2$ (**III**). The reactants were handled in a dry box under nitrogen atmosphere and loaded into fused silica ampoules. These ampoules were flame sealed under vacuum and placed in a temperature-controlled tube furnace. The furnace was ramped to 300°C at 5°C/h, maintained at this temperature for a day, and then fired at 700°C at 5°C/h for 6 days before a cooling back to room temperature in 20 h. The reactions led to the stabilization of very air sensitive, yellow crystals in a low yield (the major, observed impurities were Ln_2SbS_5Br red materials (Ln = La, Ce) (6) and SbS_3). A micropobe analysis by energy dispersive X-ray spectroscopy (EDXS) gave the chemical formula $Ce_{1.19}Sb_1S_{2.09}Br_{2.20}$, $Ce_{0.47}La_{0.51}Sb_1S_{2.10}Br_{1.81}$, and $La_{0.98}Sb_1S_{2.12}Br_{1.95}$ for **I**, **II** and **III**, respectively. No luminescence under UV radiation was observed at room temperature. So far, attempts to prepare these materials in large amounts by changing the reactant ratios and the synthesis conditions remain unsuccessful.

TABLE 1
Crystallographic and Experimental Data

		Physical and crystallographic data	
Formula	$CeSbS_2Br_2$ (I)	$La_{0.5}Ce_{0.5}SbS_2Br_2$ (II)	$LaSbS_2Br_2$ (III)
Crystal color	yellow	yellow	yellow
Molecular weight (g mol^{-1})	485.8	485.19	484.6
Crystal system		monoclinic	
Space group		$P2_1/c$ (no. 14)	
Z		4	
Cell parameters	$a = 8.709(3)$ Å	$a = 8.739(7)$ Å	$a = 8.785(1)$ Å
	$b = 9.187(2)$ Å	$b = 9.219(7)$ Å	$b = 9.236(2)$ Å
	$c = 17.397(5)$ Å	$c = 17.41(2)$ Å	$c = 17.372(3)$ Å
	$\beta = 104.26(3)°$	$\beta = 104.3(1)°$	$\beta = 104.09(2)°$
	$V = 1349(1)$ Å^3	$V = 1359(9)$ Å^3	$V = 1367(7)$ Å^3
Density (calc.)	4.782 g cm^{-3}	4.743 g cm^{-3}	4.708 g cm^{-3}
		Data collection	
Temperature		293 K	
Radiation		$\lambda_{MoK-L2,3} = 0.71069$ Å	
Diffractometer		STOE Image Plate	
Angular range 2θ (°)		3.8–56.3	
hkl range	$-11 \le h \le 11$	$-11 \le h \le 11$	$-9 \le h \le 9$
	$-11 \le k \le 11$	$-11 \le k \le 11$	$-10 \le k \le 10$
	$-22 \le l \le 22$	$-22 \le l \le 22$	$-19 \le l \le 19$
		Data reduction	
Absorption coefficient (cm^{-1})	229.98	226.63	222.87
T_{min}/T_{max}	0.17/0.40	0.22/0.34	0.19/0.33
Total recorded reflections	11251	16803	9117
Observed reflections ($I > 2\sigma(I)$)	1754	1356	1161
R_{int} (%)	5.47	8.60	8.48
		Refinement	
Refinement		F^2	
Weighting scheme		$w = 1/(\sigma^2\lvert F_o\rvert + (0.01*1.6\lvert F_o\rvert)^2)$	
No. of refined parameters		111	
Twin matrices		$\begin{pmatrix}1&0&0\\0&1&0\\0&0&1\end{pmatrix}$ $\begin{pmatrix}1&0&-1\\0&-1&0\\0&0&-1\end{pmatrix}$	
Twin fractions	72.9% 27.1(1)%	96.7 3.3(3)%	92% 8.0(2)%
Refinement results	$R(\%) = 3.50$ $Rw(\%) = 6.06$	$R(\%) = 3.87$ $Rw(\%) = 6.39$	$R(\%) = 4.25$ $Rw(\%) = 8.28$
	GOF = 0.82	GOF = 0.81	GOF = 1.24
Residual electronic density	$[-2.99, +2.73]e^-/Å^3$	$[-1.73, +1.86]e^-/Å^3$	$[-2.66, +2.73]e^-/Å^3$

X-Ray Structure Determination

Several crystals were selected in a dry box under argon atmosphere and placed into silica capillaries. Crystal screenings and intensity data collections were carried out at room temperature on a STOE Imaging Plate Diffraction System. Recording conditions are given in Table 1. Data reductions, Lorentz polarization, and crystal size and shape optimizations were performed with the STOE software package (7). Analytical absorption corrections, averaging, and all subsequent calculations, except the direct methods trials, were realized with the Jana98 programs (8). Scattering factors and anomalous dispersion correction terms were taken from Maslen *et al.* (9) and Creagh and McAuley (10), respectively.

$CeSbS_2Br_2$ (**I**): In a first stage, a C-centered lattice cell with parameters: $a \approx 8.7$ Å, $b \approx 33.8$ Å, and $c \approx 9.2$ Å was chosen, in agreement with the orthorhombic apparent symmetry of the structure. Examination of the reflections with $I > 2\sigma(I)$ revealed systematic absences compatible with the $C222_1$ noncentrosymmetric space group. A first structural model was then obtained using the Sir97 direct methods (11), and the structure refinement was initiated. However, considering the rather poor matching of the equivalent reflections within the 222 point group and the bad refinement results, a possible twinning was considered. Possible subgroups of $C222_1$, such as $P2_1$, were thus envisioned. Finally, after several attempts, $P2_1/c$ was found to be the space group giving the best results in a monoclinic cell with parameters $a = 8.709(3)$ Å, $b = 9.187(2)$ Å, $c = 17.397(5)$ Å, and $\beta = 104.26(3)^\circ$, the pseudo orthorhombic symmetry being introduced through a twofold twinning operation along the a axis. Notice that the twinning partially destroys the c mirror glide systematic absences. Starting atomic positions used for the refinement were taken from the orthorhombic initial solution. A convergence with a residual factor of $R = 0.12$ was swiftly achieved using isotropic displacement parameters (IDPs). By introducing anisotropic displacement parameters (ADPs) and refining the twinning fraction and the secondary extinction (12), a residual factor $R = 0.035$ ($Rw(F^2) = 0.061$) was easily obtained for 111 parameters and 1754 observed (2σ level) reflections. Final results are gathered in Tables 1 and 2. Anisotropic atomic displacement parameters of **I** are given as supplementary materials.

$Ce_{0.5}La_{0.5}SbS_2Br_2$ (**II**) and $LaSbS_2Br_2$ (**III**): Structure refinements were initiated from the solution obtained for $CeSbS_2Br_2$ (**I**). For $Ce_{0.5}La_{0.5}SbS_2Br_2$, the cerium and lanthanum positions could not be differentiated; therefore, a statistic occupation was introduced. Final residual R values of 0.0387 ($Rw(F^2) = 0.0639$) for 1356 reflections and 111 parameters and of 0.0425 ($Rw(F^2) = 0.0828$) for 1161 reflections and 111 parameters were achieved for **II** and **III**, respectively. Both studied crystals were also twinned, but with in each case a predominant domain (96.7(3)% and 92.0(2)%, respectively). Final results are gathered in Tables 1 and 2. Anisotropic atomic displacement parameters of **II** and **III** are given as supplementary materials.

Optical Spectroscopy

Room-temperature optical diffuse reflectance spectra in the 400–800 nm (1.5–3.1 eV) range were obtained using

TABLE 2

Fractional Atomic Coordinates and Equivalent Isotropic Atomic Displacement Parameter of (a) $CeSbS_2Br_2$, (b) $Ce_{0.5}La_{0.5}SbS_2Br_2$, and (c) $LaSbS_2Br_2$

Atom	Wyckoff position	τ	x	y	z	ADP_{eq}(Å^2)
				(a)		
Ce(1)	4*e*	1	0.3865(1)	0.8623(1)	0.76366(5)	0.98(2)
Ce(2)	4*e*	1	0.8780(2)	0.8668(1)	0.75553(5)	1.19(2)
Sb(1)	4*e*	1	0.2739(2)	0.1573(1)	0.55450(6)	1.43(3)
Sb(2)	4*e*	1	0.7296(2)	0.0441(1)	0.95235(7)	1.44(3)
S(1)	4*e*	1	0.0737(5)	0.3498(6)	0.5525(2)	1.4(1)
S(2)	4*e*	1	0.3396(7)	0.1628(4)	0.6968(2)	1.2(1)
S(3)	4*e*	1	0.6639(7)	0.0628(4)	0.8096(2)	1.1(1)
S(4)	4*e*	1	0.4757(5)	0.3486(6)	0.5533(3)	1.6(1)
Br(1)	4*e*	1	0.5547(3)	0.8715(2)	0.62805(9)	1.62(5)
Br(2)	4*e*	1	0.0782(3)	0.8690(2)	0.63334(9)	1.61(4)
Br(3)	4*e*	1	0.1570(3)	0.6722(2)	0.8341(1)	1.52(5)
Br(4)	4*e*	1	0.8378(3)	0.5575(2)	0.6596(1)	1.34(5)
				(b)		
Ce(1)	4*e*	0.5	0.3864(1)	0.8630(2)	0.76355(8)	0.82(3)
La(1)	4*e*	0.5	0.3864	0.8630	0.76355	0.82
Ce(2)	4*e*	0.5	0.8777(1)	0.8682(2)	0.75564(8)	0.95(4)
La(2)	4*e*	0.5	0.8777	0.8682	0.75564	0.95
Sb(1)	4*e*	1	0.2735(2)	0.1580(2)	0.5543(1)	1.28(5)
Sb(2)	4*e*	1	0.7300(2)	0.0437(2)	0.9528(1)	1.20(5)
S(1)	4*e*	1	0.0746(6)	0.3500(9)	0.5525(3)	1.4(1)
S(2)	4*e*	1	0.3386(7)	0.1642(8)	0.6966(4)	0.8(2)
S(3)	4*e*	1	0.6631(7)	0.0630(8)	0.8110(5)	1.2(2)
S(4)	4*e*	1	0.4748(6)	0.3485(8)	0.5534(4)	1.4(1)
Br(1)	4*e*	1	0.5552(3)	0.8729(4)	0.6281(1)	1.52(7)
Br(2)	4*e*	1	0.0786(2)	0.8706(4)	0.6332(1)	1.41(7)
Br(3)	4*e*	1	0.1578(3)	0.6734(3)	0.8346(2)	1.37(8)
Br(4)	4*e*	1	0.8379(3)	0.5588(3)	0.6595(2)	1.38(8)
				(c)		
La(1)	4*e*	1	0.3861(2)	0.8649(2)	0.76335(7)	0.99(3)
La(2)	4*e*	1	0.8776(2)	0.8699(2)	0.75546(7)	1.15(3)
Sb(1)	4*e*	1	0.2731(2)	0.1602(2)	0.55396(9)	1.44(4)
Sb(2)	4*e*	1	0.7304(3)	0.0446(2)	0.9536(1)	1.45(4)
S(1)	4*e*	1	0.0734(7)	0.3516(7)	0.5520(3)	1.3(1)
S(2)	4*e*	1	0.3394(8)	0.1660(6)	0.6960(4)	1.1(2)
S(3)	4*e*	1	0.6632(8)	0.0655(6)	0.8117(4)	1.2(2)
S(4)	4*e*	1	0.5270(7)	−0.1493(7)	0.9481(3)	1.4(1)
Br(1)	4*e*	1	0.5549(3)	0.8753(3)	0.6274(1)	1.66(6)
Br(2)	4*e*	1	1.0776(3)	0.8724(3)	0.6321(1)	1.58(6)
Br(3)	4*e*	1	0.1579(4)	0.6756(2)	0.8348(1)	1.56(7)
Br(4)	4*e*	1	0.8385(4)	0.5607(3)	0.6593(1)	1.52(7)

a Leitz system (DM RXP metallographic microscope coupled with a MPV spectrophotometer) and MgO (Prolabo) as a reference (100% reflectance). Crystals deposited on a glass side were positioned over the light source and the reflected light was detected from above. Experiments were carried out in oil (Aldrich) to prevent the studied materials from deterioration. The absorption data (α/S) were calculated from the reflectance using the Kubelka–Munk function (13–15) $\alpha/S = (1-R)^2/2R$, where R is the reflectance at a given energy, α is the absorption, and S is the scattering coefficient. The energy gap was determined as the intersection point between the energy axis at the absorption offset and the line extrapolated from the linear portion of the absorption edge in the α/S versus E(eV) plot.

Band Structure Calculations

TB–LMTO electronic band structure calculations were carried out for $CeSbS_2Br_2$ and $LaSbS_2Br_2$ in the atomic sphere approximation using the LMTO47 program (16–19). Due to the high similarities between the band structures of these materials, only results on $CeSbS_2Br_2$ are reported here. Exchange and correlation were treated in a local spin density approximation (20). All the relativistic effects except the spin–orbit coupling were taken into account using a scalar relativistic approximation (21).

In the atomic sphere approximation, the space is filled with small overlapping Wigner–Seitz (WS) atomic spheres. The symmetry of the potential is considered spherical inside each WS sphere, and a combined correction is used to take into account the overlapping part (22). The radii of the WS spheres were obtained by requiring that the overlapping potential be the best possible approximation to the full potential, and they were determined by an automatic procedure described in Ref. (22). This overlap should not be too large because the error in the kinetic energy introduced by the combined correction is proportional to the 4th power of the relative sphere overlap. The interatomic space was filled with interstitial spheres since the structures of the compound under examination are not closely packed. The optimal positions and radii (r_{ES}) of these "empty spheres" were determined according to the method described in (22). For calculations on $CeSbS_2Br_2$, 22 empty spheres with 0.82 Å $\leq r_{ES} \leq$ 1.84 Å were introduced. This made the maximum relative overlap between two adjacent atomic spheres less than 16%. The positions and radii of the WS spheres used are given as supplementary materials.

The basis set included Ce–6*s*, 5*d* and 4*f* orbitals, Sb–5*s* and 5*p* orbitals, S–3*s* and 3*p* orbitals, and Br–4*p* orbitals. We used *s* orbitals for the empty spheres. The Ce–6*p* orbitals, the Sb–5*d* and 4*f* orbitals, the S–3*d* orbitals, the Br–5*s* and 4*d* orbitals, and, depending on the size of the WS empty spheres, the *p* and *d* or only *p* orbitals were treated by the Löwdin downfolding technique (16–19). The k-space integrations were performed by the tetrahedron method (23). The self-consistent charge density was obtained using 30 irreducible k points. The contribution of the nonspherical part of the charge density to the potential was neglected.

RESULTS AND DISCUSSIONS

Structure Description

I, **II**, and **III** are isostructural and exhibit a novel, 2D structural arrangement. The structure is made of distorted tricapped trigonal prisms [$Ln(1)S_4Br_2$, SBr_2] and [$Ln(2)S_2Br_4$, SBr_2] (Ln = Ce, La) (see Figs. 1a and 1b) with Ln–S and Ln–Br distances in the expected range for Ln^{III}–S^{-II} and Ln^{III}–Br^{-I} bonds (see Table 3). The aforementioned $Ln(1)$ and $Ln(2)$ polyhedra share one S–S and one Br–Br edge, respectively, of their basal triangular face to form infinite $^1_\infty[Ln(1)_2S_6Br_8]$ and $^1_\infty[Ln(2)_2S_6Br_8]$ chains running along the *b* axis (see Figs. 2a and 2b). These chains condense to give rise to infinite corrugated $^2_\infty[Ln(1)Ln(2)S_4Br_4]$ layers

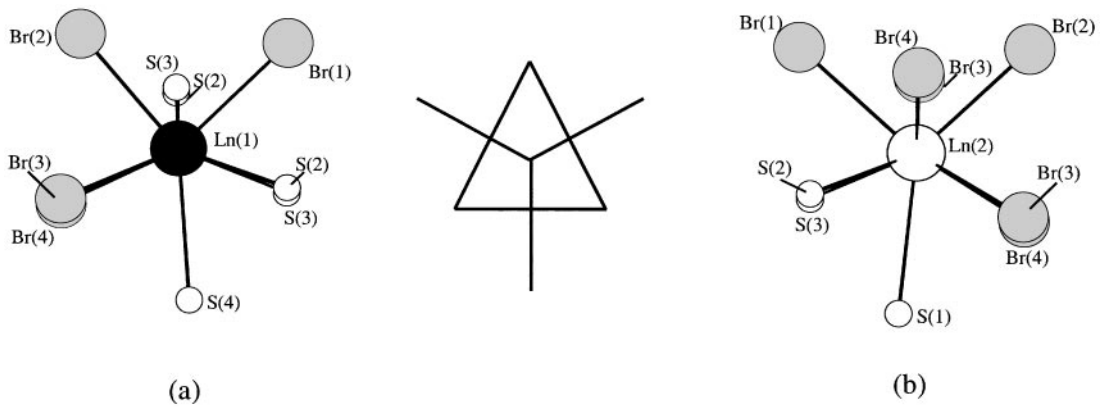

FIG. 1. (a) [$Ln(1)S_4Br_2$,SBr_2] and (b) [$Ln(2)S_2Br_4$,SBr_2] polyhedra constituting the building blocks of the $Ln SbS_2Br_2$ phases with the labeling scheme (Ln = Ce, La).

TABLE 3
Selected Bond Distances (Å) and Angles (°) in (a) $CeSbS_2Br_2$, (b) $Ce_{0.5}La_{0.5}SbS_2Br_2$, and (c) $LaSbS_2Br_2$

		(a)	
$[Ce(1)S_5Br_4]$ polyhedron		$[Ce(2)S_3Br_6]$ polyhedron	
Ce(1)–S(2)	2.984(4)	Ce(2)–S(1)	3.266(4)
Ce(1)–S(2)	2.952(5)	Ce(2)–S(2)	2.926(6)
Ce(1)–S(3)	2.986(5)	Ce(2)–S(3)	2.909(6)
Ce(1)–S(3)	3.019(4)	Ce(2)–Br(1)	3.126(2)
Ce(1)–S(4)	3.117(4)	Ce(2)–Br(2)	3.064(3)
Ce(1)–Br(1)	3.069(2)	Ce(2)–Br(3)	3.055(2)
Ce(1)–Br(2)	3.059(2)	Ce(2)–Br(3)	3.188(2)
Ce(1)–Br(3)	3.123(3)	Ce(2)–Br(4)	3.271(2)
Ce(1)–Br(4)	3.179(3)	Ce(2)–Br(4)	3.094(2)
Average values			
Ce(1)–S	3.012	Ce(2)–S	3.034
Ce(1)–Br	3.108	Ce(2)–Br	3.133
$[SbS_3Br_4]$ polyhedron		$[SbS_5Br_3]$ polyhedron	
Sb(1)–S(1)	2.478(5)	Sb(2)–S(1)	2.490(5)
Sb(1)–S(2)	2.401(4)	Sb(2)–S(3)	2.414(4)
Sb(1)–S(4)	2.489(5)	Sb(2)–S(4)	2.519(5)
Average values			
Sb(1)–S	2.456	Sb(2)–S	2.474
		(b)	
$[Ln(1)S_5Br_4]$ polyhedron		$[Ln(2)S_3Br_6]$ polyhedron	
Ln(1)–S(2)	3.000(7)	*Ln*(2)–S(1)	3.266(6)
Ln(1)–S(2)	2.964(7)	*Ln*(2)–S(2)	2.929(7)
Ln(1)–S(3)	2.990(7)	*Ln*(2)–S(3)	2.927(8)
Ln(1)–S(3)	3.040(8)	*Ln*(2)–Br(1)	3.127(2)
Ln(1)–S(4)	3.119(6)	*Ln*(2)–Br(2)	3.079(3)
Ln(1)–Br(1)	3.077(3)	*Ln*(2)–Br(3)	3.072(3)
Ln(1)–Br(2)	3.060(2)	*Ln*(2)–Br(3)	3.200(3)
Ln(1)–Br(3)	3.130(3)	*Ln*(2)–Br(4)	3.281(4)
Ln(1)–Br(4)	3.193(4)	*Ln*(2)–Br(4)	3.103(3)
Average values			
Ln(1)–S	3.023	*Ln*(2)–S	3.041
Ln(1)–Br	3.115	*Ln*(2)–Br	3.142
$[SbS_3Br_4]$ polyhedron		$[SbS_5Br_3]$ polyhedron	
Sb(1)–S(1)	2.475(7)	Sb(2)–S(1)	2.489(7)
Sb(1)–S(2)	2.401(7)	Sb(2)–S(3)	2.399(8)
Sb(1)–S(4)	2.489(7)	Sb(2)–S(4)	2.521(7)
Average values			
Sb(1)–S	2.455	Sb(2)–S	2.470
		(c)	
$[La(1)S_5Br_4]$ polyhedron		$[La(2)S_3Br_6]$ polyhedron	
La(1)–S(2)	3.008(6)	La(2)–S(1)	3.272(5)
La(1)–S(2)	2.976(6)	La(2)–S(2)	2.945(7)
La(1)–S(3)	3.011(7)	La(2)–S(3)	2.943(7)
La(1)–S(3)	3.044(6)	La(2)–Br(1)	3.149(3)
La(1)–S(4)	3.144(5)	La(2)–Br(2)	3.084(3)
La(1)–Br(1)	3.086(3)	La(2)–Br(3)	3.087(3)
La(1)–Br(2)	3.091(2)	La(2)–Br(3)	3.208(3)
La(1)–Br(3)	3.131(3)	La(2)–Br(4)	3.283(3)
La(1)–Br(4)	3.199(3)	La(2)–Br(4)	3.118(3)
Average values			
La(1)–S	3.036	La(2)–S	3.053
La(1)–Br	3.127	La(2)–Br	3.155
$[SbS_3Br_4]$ polyhedron		$[SbS_5Br_3]$ polyhedron	
Sb(1)–S(1)	2.484(7)	Sb(2)–S(1)	2.498(7)
Sb(1)–S(2)	2.394(6)	Sb(2)–S(3)	2.399(6)
Sb(1)–S(4)	2.492(7)	Sb(2)–S(4)	2.515(7)
Average values			
Sb(1)–S	2.457	Sb(2)–S	2.471

running in the (*a*, *b*) plane (see Fig. 3a) and are capped by threefold coordinated antimony cations defining $[SbS_3]$ trigonal pyramids (Sb–S bonds around 2.46 Å). The cohesion of the tridimensional edifice (see Fig. 3b) is mainly ensured by van der Waals interactions between $^2_\infty[LnSbS_2Br_2]$ slabs with possible long-range Sb–S and Sb–Br interactions (Sb–S and Sb–Br distances across the van der Waals gap are higher than 3.2 and 3.6 Å, respectively).

Because of the well-known stability of Ce^{III} and La^{III} in chalcogenides, and of the Sb^{III} environment characteristic of the existence of a $5s^2$ lone pair, the charge balance of the phase must be written $Ln^{III}Sb^{III}S_2^{-II}Br_2^{-I}$.

Optical Properties

I, **II**, and **III** crystals exhibit a hue ranging from bright to pale yellow. To determine quantitatively the energy gap responsible for the color in these compounds and to shed light on the electronic transition at work, diffuse reflectance experiments were undertaken on single crystals. The obtained α/S vs energy spectra, reported in Fig. 4, show an absorption threshold at 2.42(1) eV for $CeSbS_2Br_2$, 2.55(1) eV for $Ce_{1/2}La_{1/2}S_2Br_2$, and 2.72(1) eV for

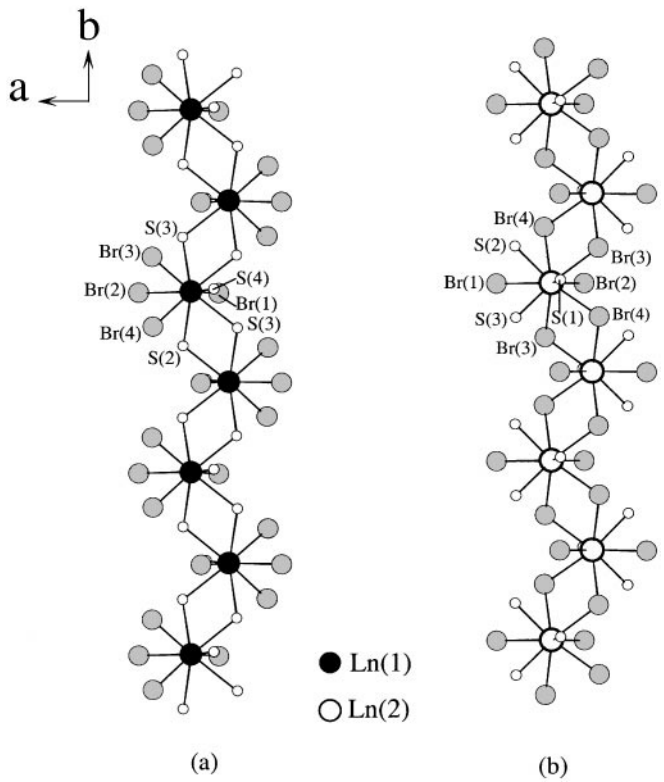

FIG. 2. Arrangements of the (a) $[Ln(1)S_4Br_2,SBr_2]$ and (b) $[Ln(2)S_2Br_4,SBr_2]$ polyhedra into $^1_\infty[Ln(1)_2S_6Br_8]$ and $^1_\infty[Ln(2)_2S_6Br_8]$ infinite chains running along the *b* axis.

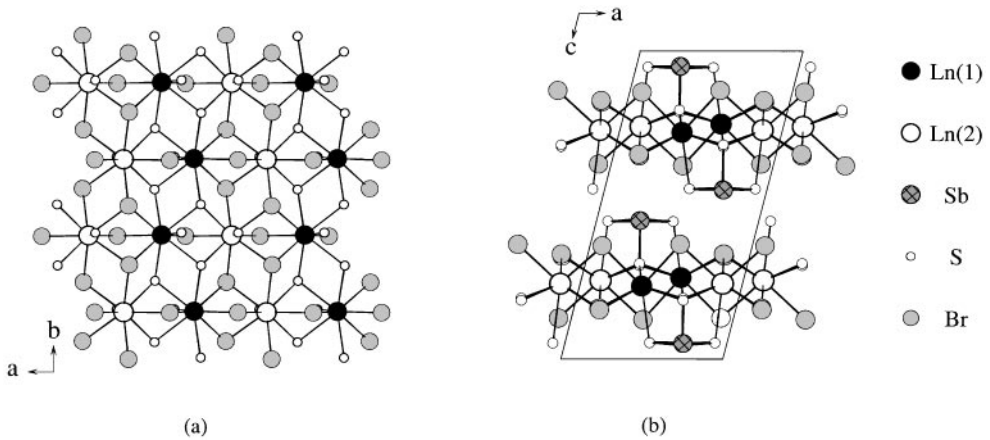

FIG. 3. (a) View perpendicular to the (a, b) plane of the $^2_\infty[Ln(1)\ Ln(2)S_4Br_4]$ layers resulting from the condensation of $^1_\infty[Ln(1)_2S_6Br_8]$ and $^1_\infty[Ln(2)_2S_6Br_8]$ infinite chains (Ln = Ce, La). (b) View perpendicular to the (a, c) plane of the $^2_\infty[LnSbS_2Br_2]$ layers showing the corrugated van der Waals gap.

$LaSbS_2Br_2$. The interference pattern observed below the band gap only results from the finite thickness of the specimens and their refractive index relative to oil.

At this stage, a first discussion on the origin of the optical properties may be given. For $LaSbS_2Br_2$, the color of the phase can only stem from an electronic transition from the top of the valence band (VB) to the bottom of the conduction band (CB). As La is substituted for Ce, localized Ce–4*f* levels are interspaced between the valence band and the conduction band, inducing a significant lowering of the absorption threshold energy (from 2.72(1) eV for **III** to 2.42(1) eV for **I**, for instance). Moreover, the shift from 2.42(1) eV for $CeSbS_2Br_2$ (**I**) to 2.55(1) eV for $Ce_{1/2}La_{1/2}SbS_2Br_2$ (**II**) shows a quite large amplitude. A rather constant threshold value was expected (4, 25). Two explanations for the energy shift come to mind: a matrix effect or an ordering between the Ce and La atoms on the Ln(1) and Ln(2) crystallographic sites in **II**. In the first hypothesis, a random occupancy of Ce and La atoms on Ln(1) and Ln(2) sites is implied. Then, because Ce–S and Ce–Br distances are longer in $Ce_{1/2}La_{1/2}SbS_2Br_2$ than in $CeSbS_2Br_2$ (see Table 3a and 3b), a wider 4*f*–5*d* separation is expected for $Ce_{1/2}La_{1/2}S_2Br_2$ due to an increase of the Ce–ligand bond ionicity. However, EXAFS experiments and diffuse reflectance measurements made on the $Y_{1-x}Ce_xPS_4$ solid (24) solution showed that the cerium cations keep the characteristics of the chemical surrounding they have in $CePS_4$, irrespective of the Y/Ce ratio. As a result, there is no change at all in the energy position of the Ce–4*f* → Ce–5*d* absorption threshold versus the Ce concentration in the solid solution. Thus, the occurrence of a matrix effect in the bromothioantimonates of cerium and lanthanum may be *a priori* ruled out. In the second hypothesis, we may consider, as observed in $La_{2.999}Ce_{0.001}(SiS_4)_2I$ at 6 K (2), that the two Ln(1) and Ln(2) sites of the structure give two different $4f \rightarrow 5d$ transition energies occurring at 2.42(1) or 2.55(1) eV. The increase in the absorption threshold from **I** to **II** would then originate in a preferential occupation by Ce cations of Ln(1) or Ln(2) crystal sites, resulting consequently in an ordering between cerium and lanthanum in **II**.

Band Structure Calculations

Band structure calculations on **I** and **III** were carried out. For clarity, only results on $CeSbS_2Br_2$ are reported here. The results on the La derivative can be straightforwardly deduced from those of Ce_2SbS_5Br by removal of the 4*f* block from the VB–CB energy gap.

The total density of states (DOS) for $CeSbS_2Br_2$ in the $[-3, +3]$ eV energy range is displayed in Fig. 5, along with the atomic contributions. The calculated band dispersion is given as supplementary materials for the k Bloch vectors along the ΓZ, ΓB, ΓY symmetry lines of the reciprocal space. The zero energy is taken at the Fermi level.

In the $[-3, +3]$ eV energy range, the DOS curve can be separated into three regions. The valence band extends up to −1.89 eV, the conduction band lies above 0.68 eV, and in between is located the Ce–4*f* block. The topmost levels of the VB are mainly built upon bromine contribution but contain a sulfur contribution as well. The first unoccupied levels of the CB is antimony in character, the Ce–*d* orbitals participating significantly to the DOS only at energies higher than 0.89 eV. Consequently the VB → CB electronic transition is not assigned to a S, Br → 5*d*–Ce charge transfer as it could be expected, but rather to a S, Br → Sb transfer (it is this transition (at 2.72 eV) that gives $La_2SbS_2Br_2$ its pale yellow color).

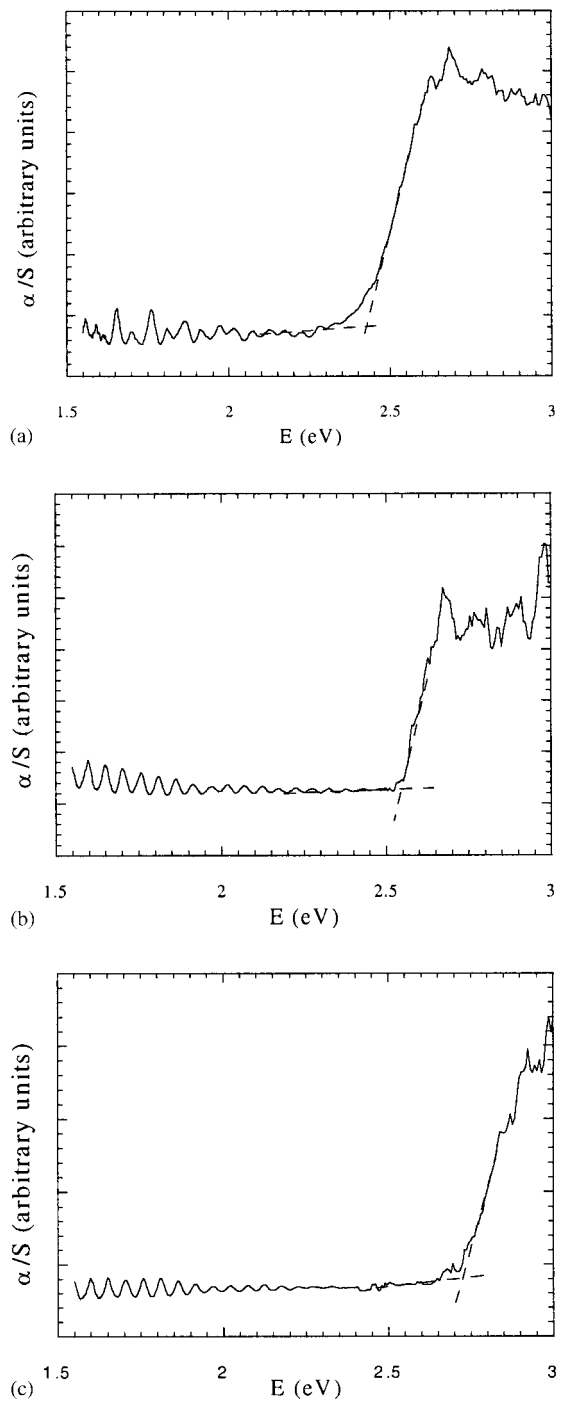

FIG. 4. Single-crystal absorption spectra of (a) $CeSbS_2Br_2$, (b) $Ce_{1/2}La_{1/2}SbS_2Br_2$, and (c) $LaSbS_2Br_2$.

The Fermi level lies within the Ce–4*f* block. A high density of states is calculated around E_f in relation with a very low dispersion of the Ce–4*f* levels connected to a small space extension of the *f* orbitals and to the lack of any meaningful hybridization. Even if this band is only 1/14th filled, no electronic conductivity may arise due to the occurrence of a high $4f^1 + 4f^1 \rightarrow 4f^0 + 4f^2$ Hubbard term ($\sim$6 eV) not taken into account in the calculation. Hence, owing to the high energy cost required to add an extra electron to Ce^{III}, only the promotion of electrons from the 4*f* block (and from the VB toward the CB as seen above) may occur under light excitation. At this stage, we must remind that the energy position of the Ce–*f* block is not accurately positioned because of the difficulty to take into account the localized *f*-orbital character in a band-like approach.

Owing to the common intrasite character of transitions implying the promotion of a Ce^{III}–$4f^1$ electron, a $Ce^{III} \rightarrow Sb^{III}$ charge transfer (i.e., a Ce–$4f \rightarrow$ CB bottom transition) appears highly improbable. Thus, the color in $CeSbS_2Br_2$ and $Ce_{1/2}La_{1/2}SbS_2Br_2$ should be due to the spin and symmetry allowed intrasite Ce–$4f \rightarrow$ Ce–5*d* electronic transition, whereas the VB $\rightarrow$ CB transition is taking place at higher energy (even if the Sb–5*p* levels lie lower in energy than the Ce–5*d* levels) and contribute marginally to the color. The features of the electronic band structures of $LaSbS_2Br_2$ are quite comparable to those of $CeSbS_2Br_2$ with an identical VB–CB gap within the error (less than 0.1 eV difference).

The color mechanisms at work in $CeSbS_2Br_2$, can then be schemed as shown in Fig. 6a, where the atomic contributions to the total density of states have been reinforced in order to gain clarity. Hence, $CeSbS_2Br_2$ is characterized by a Ce–$4f \rightarrow$ Ce–5*d* transition taking place at an energy smaller than the VB $\rightarrow$ CB and by a CB bottom built on antimony orbitals. In contrast, $Ce_3(SiS_4)_2I$ (1) (see Fig. 6b) evidences similar electronic transitions with a Ce–$4f \rightarrow$ Ce–5*d* transition smaller in energy than the VB $\rightarrow$ CB but with a CB bottom built on Ce–5*d* orbitals. These two models are still different from the coloring process observed in $Ce_2Sb(S_2)S_3Br$ (6), where color does not originate from a too high in energy Ce–$4f \rightarrow$ Ce–5*d* electronic transition but from a charge transfer from unpaired S and/or Br atoms toward Sb and/or paired S atoms as sketched in Fig. 6c. Hence, even in Ce^{III}-containing phases with an allowed, favorable Ce–$4f \rightarrow$ Ce–5*d* electronic transition, the origins of color may be quite diverse.

CONCLUSION

Crystals of $LnSbS_2Br_2$ (Ln = Ce, La) have been synthesized and characterized. These new materials, containing distorted tricapped trigonal prisms $[Ln(1)S_5Br_4]$ and $[Ln(2)S_3Br_6]$, crystallize in a novel structural type and exhibit a hue ranging from bright yellow ($CeSbS_2Br_2$) to pale yellow ($LaSbS_2Br_2$). This color change is to be related to different absorption mechanisms, inducing modifications in the absorption threshold position. While the color originates from a Ce–$4f \rightarrow$ Ce–5*d* electronic transition in

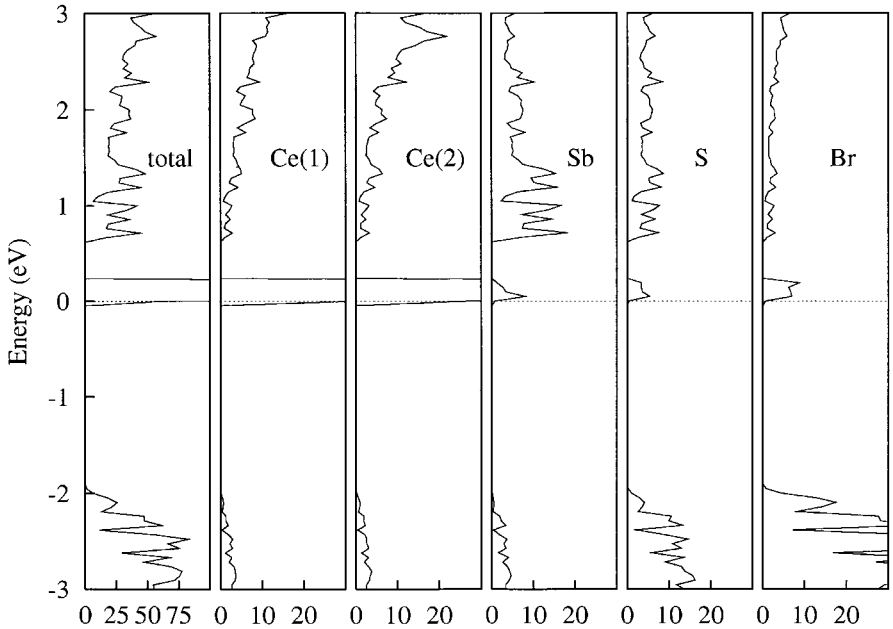

FIG. 5. Total density of states (DOS) of $CeSbS_2Br_2$ and DOS projected along the different elements between -3 and $+3$ eV.

$CeSbS_2Br_2$ and $Ce_{1/2}La_{1/2}SbS_2Br_2$, a higher energy S^{-II}, $Br^{-I} \rightarrow Sb^{III}$ charge transfer occurs in $LaSbS_2Br_2$. The small energy difference in the absorption threshold observed between $CeSbS_2Br_2$ and $Ce_{1/2}La_{1/2}SbS_2Br_2$ is supposed to stem from the intrasite character of the Ce–4*f* → Ce–5*d* transition, the 2.42(1) and 2.55(1) eV optical gaps being assigned to absorption phenomena occurring on specific crystallographic sites (Ce(1) and Ce(2) sites or Ce(2) and Ce(1) sites, respectively). These results show that the color of compounds originate in varied electronic transitions in complex phases. In particular, they demonstrate that it is difficult to put forward simple, *a priori* mechanisms derived from previously studied materials. For instance, the well documented, often occurring Ce–4*f* → Ce–5*d* transition may not take place in quaternary compounds because of the nature of the bottom/top of the electronic bands.

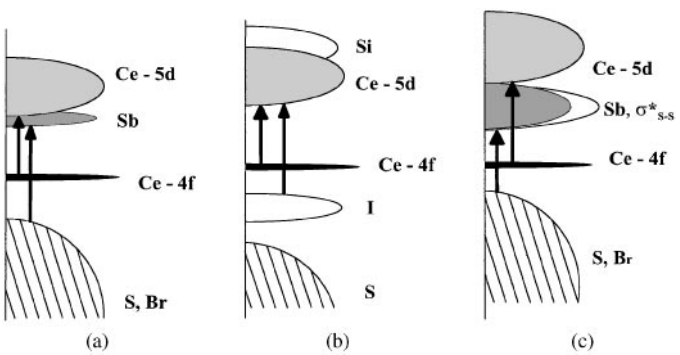

FIG. 6. Schematic representation of the different electronic transitions involved in (a) $CeSbS_2Br_2$, (b) $Ce_3(SiS_4)_2I$, and (c) $Ce_2Sb(S_2)S_3Br$, and responsible for the color of the phases.

REFERENCES

1. G. Gauthier, S. Kawasaki, S. Jobic, P. Macaudière, R. Brec, and J. Rouxel, *J. Mater. Chem.* **8,** 179 (1998).
2. R. Riccardi, D. Gout, G. Gauthier, F. Guillen, S. Jobic, A. Garcia, D. Huguenin, P. Macaudière, C. Fouassier, and R. Brec, *J. Solid State Chem.* **147,** 259 (1999).
3. J. Etourneau, J. Portier, and F. Ménil, *J. Alloys Compd.* **188,** 1 (1992).
4. G. Gauthier, S. Jobic, F. Boucher, P. Macaudière, D. Huguenin, J. Rouxel, and R. Brec, *Chem. Mater.* **10,** 2341 (1998).
5. G. Gauthier, S. Jobic, P. Macaudière, and R. Brec, *Mater. Res. Soc. Symp. Proc.* **548,** 667 (1999).
6. D. Gout, S. Jobic, M. Evain, and R. Brec, *Solid State Sci.*, in press (2001).
7. Stoe software (1996), Stoe & Cie Gmbh, Darmstadt, Germany.
8. V. Petricek and M. Dusek, "JANA98: Programs for Modulated and Composite Crystals." Institute of Physics, Praha, Czech Republic, 1998.
9. E. N. Maslen, A. G. Fox, and M. A. O'Keefe, "International Tables for X-Ray Crystallography: Vol. C, Mathematical, Physical and Chemical Tables" (A. J. C. Wilson, Ed.), Ch. 6.1. Kluwer Academic, Dordrecht, 1992.
10. D. C. Creagh and W. J. McAuley, "International Tables for X-Ray Crystallography: Vol. C, Mathematical, Physical and Chemical Tables" (A. J. C. Wilson, Ed.), Ch. 4.2. Kluwer Academic, Dordrecht, 1992.
11. A. Altomare, G. Cascarano, C. Giacovazzo, A. Guagliardi, A. G. G. Moliterni, M. C. Burla, G. Polidori, M. Camalli, and R. Spagna, "Sir97: A Package for Crystal Structure Solution by Direct Methods and Refinement." Italy, 1997.
12. P. J. Becker and P. Coppens, *Acta Crystallogr. Sect. A*: *Found. Crystallogr.* **30,** 129 (1974).
13. W. W. Wendlandt and H. G. Hecht, "Reflectance Spectroscopy." Interscience, New York, 1966.
14. G. Kortüm, "Reflectance Spectroscopy." Springer-Verlag, Berlin/New York, 1969.
15. S. P. Tandon and J. P. Gupka, *Status Solidi*, 363 (1970).

16. O. K. Andersen, *Phys. Rev. B* **12,** 3060 (1975).
17. O. K. Andersen and O. Jepsen, *Phys. Rev. Lett.* **53,** 2571 (1984).
18. O. K. Andersen, O. Jepsen, and D. Glötzel, "Highlights of Condensed-Matter Theory" (F. Bassani, F. Fumi, and M. P. Tosi, Eds.). North-Holland, Lambrecht, W. R. L., 1985.
19. O. K. Andersen, *Phys. Rev. B* **34,** 2439 (1986).
20. U. von Barth and L. Hedin, *J. Phys. C* **5,** 1629 (1972).
21. D. Koelling and B. N. Harmon, *J. Phys. C* **10,** 3107 (1977).
22. O. Jepsen and O. K. Andersen, *Z. Phys. B* **97,** 345 (1995).
23. P. E. Blöchl, O. Jepsen, and O. K. Andersen, *Phys. Rev. B* **49,** 16,223 (1994).
24. G. Gauthier, Y. Klur, A. Pourpoint, S. Jobic, G. Ouvrard, R. Brec, D. Huguenin, and P. Macaudière, *Int. J. Inorg. Mater.* **2,** 717 (2000).